

Contribution to the study of optical functions for signal regeneration in high-bit-rate transmission systems

Quang Trung LE
English summary of thesis

June 15, 2010

1 Introduction

Future optical high-bit-rate and long-haul links will need simple and cost-effective devices to replace some of the existing optoelectronic repeaters to enhance their performance and reduce their cost. All-optical solutions would be good candidates. In the present thesis, we propose theoretical and experimental studies of all-optical regeneration for optical transmission systems.

A key component is the microcavity saturable absorber (SA), which is particularly interesting for this type of application. This thesis investigates SA-based all-optical regeneration, and provides the following contributions:

1. The first pigtailed SA has been implemented with eight independent channels using a simple coupling technique. The device homogeneity and wideband functionality is measured. The wavelength tunability of a 2R regenerator using this type of SA and a fibre-based power limiter is studied numerically and demonstrated experimentally.
2. An alternative solution for power limiter function, based on a novel SA, is used to replace the fibre-based one. A complete 2R regenerator using a tandem of saturable absorption chips is proposed. The capacity of the regenerator for noise suppression and Q-factor enhancement, as well as the obtainable sensitivity margin at 42.7 Gbit/s, is presented. The device cascadability is shown and discussed.
3. A 3R regenerator based on a combination of a 2R regenerator and synchronous modulation is then studied. The 2R regeneration is realised by an SA and a fibre-based power limiter. The clock recovery is

based on self-pulsating semiconductor lasers. All-optical synchronous modulation is obtained by cross absorption modulation in the SA. The regenerator performance is demonstrated in a recirculating loop experiment.

4. Phase-preserving amplitude regeneration of a phase-encoded signal is studied in the last section. The novel power limiter SA is used for amplitude regeneration of return-to-zero differential phase shift keying signals. We demonstrate that, by strongly reducing the amplitude noise, which is the origin of SPM-induced nonlinear phase noise, the system performance can be improved.

2 Saturable absorber for WDM-compatible 2R regeneration

An SA is a vertical semiconductor quantum-well structure embedded in a microcavity. The device is of great interest for all-optical regeneration because of its capacity and performance. Firstly, the SA provides an efficient and completely passive solution for extinction ratio enhancement at bit rates as high as 160 Gbit/s [1]; secondly, simultaneous regeneration of several WDM channels has been shown, with spatial demultiplexing [2]. Finally, some WDM compatible solutions have been developed to fully reshape the signal at 10 Gbit/s [3].

In this work, we assess the first pigtailed SA device with 8 independent channels. Component homogeneity and spectral functionality are evaluated through switching contrast measurements. Cascadability and wavelength tunability are experimentally studied at 42.7 Gbit/s in a recirculating loop.

2.1 Module fabrication

The saturable absorber chip contains 7 InGaAs-InP quantum wells embedded in a microcavity (Figure 1). The quantum wells are located at the antinodes of intracavity intensity. The bottom mirror is a broadband high-reflectivity metallic-based mirror (Ag) and the top mirror is a multilayer dielectric mirror (2 [TiO₂-SiO₂]). Heavy-ion-irradiation shortens the absorption recovery time down to 5 ps. The device operates in a reflective mode, the reflectivity being low at low signal level, and high at high signal level. More details on the device fabrication can be found in the reference [4].

A special micro-lensed fibre array has been developed for efficiently interfacing the SA chip to 8 standard single mode fibres with 250 μm spacing

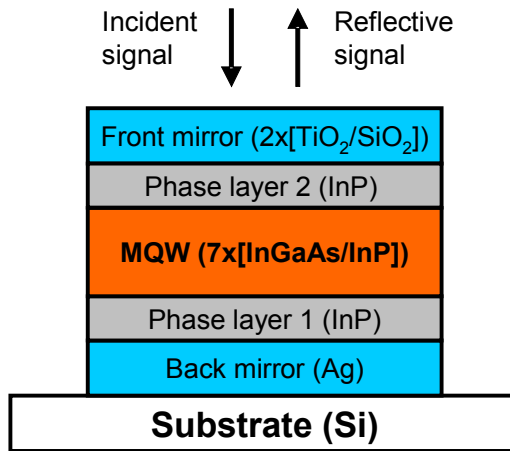


Figure 1: Microcavity saturable absorber structure.

(Figure 2). The fibre array is fixed to the mirror with an UV adhesive so that all the 8 incoming beams typically have a mode field diameter of $4.5 \mu\text{m}$ on the surface of the mirror. Focusing the beams on the mirror reduces the input power threshold required for the nonlinear effect of the mirror. This compact and low cost technique does not need any coupling optimisation.

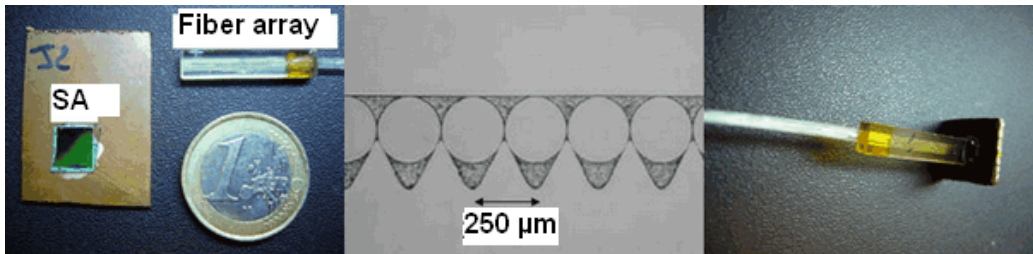


Figure 2: Saturable absorber chip and eight-fibre array used for coupling.

2.2 Module characterisation

Figure 3 presents the switching contrast of each channel as a function of average incident power and of probe wavelength obtained with classical pump-probe measurement. The pump at 1532 nm is a RZ (33%) signal modulated at 42.7 Gbit/s with sequence length of $2^{15}-1$ bit.

The first experiment, presented in Figure 3.(a), depicts the measured switching contrast versus the average incident power for each channel. The probe is delivered by a CW laser source at 1546.6 nm corresponding to the

minimum reflectivity of the SA module. With a high input pump signal power level, the probe beam is cross modulated by the SA absorption. The switching contrast is obtained from the measurement of the mark-space extinction ratio of the probe signal. It corresponds to the extinction ratio enhancement in regeneration applications. For an input pump signal power of 12 dBm, the average switching contrast is 5.5 dB on all channels with a standard deviation of 0.9 dB. This result shows the very good homogeneity of the component.

The second experiment, presented in Figure 3.(b), depicts the measured switching contrast versus the probe wavelength for each channel. The pump power is equal to 8 dBm. We observe a switching contrast higher than 3 dB over 18 nm (from 1541 nm to 1559 nm) for all channels. This shows that the module is functional over a very wide-band signal spectrum, and thus constitutes potentially a good candidate for WDM regeneration.

However, the SA alone can not perform a complete 2R regeneration function. Indeed, as the device's reflectivity increases when the input power increases, then the stronger the pulse is, the better it is reflected by the SA. As a result, amplitude fluctuations on the high level are increased after passing through the SA. Therefore, a complementary function, that is to say a power limiter, must be used. In this section, we use a fibre-based power limiter to perform complete 2R regeneration, thus validating the WDM compatibility of the SA module.

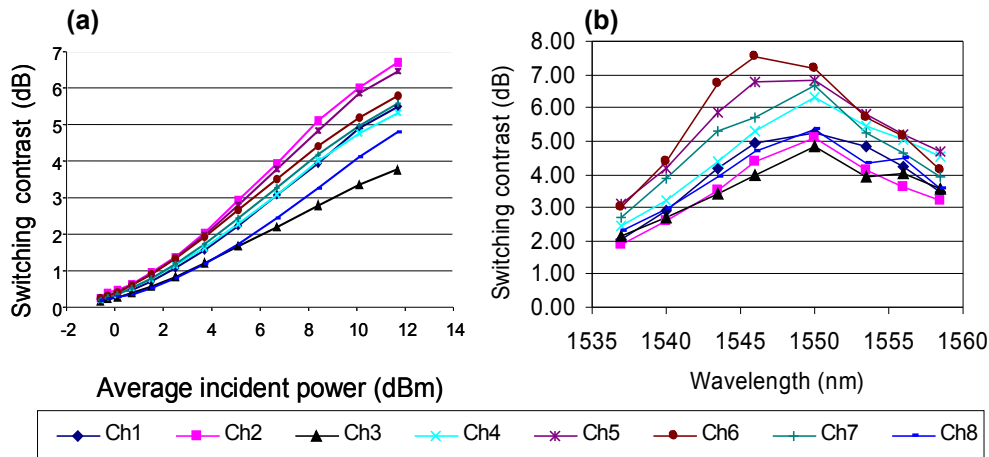


Figure 3: Experimental switching contrast of SA module against input power (a) and probe wavelength (b).

2.3 System characterisation

2.3.1 Experimental setup

The 42.7 Gbit/s transmission experiment is carried out with a 100 km long recirculating loop (Figure 4). The transmitter produces an RZ (33%) signal modulated at 42.7 Gbit/s with a $2^{31}-1$ bit length sequence. Non-zero dispersion shifted fibre (NZ DSF) is used and the chromatic dispersion is partially compensated for by a dispersion compensating fibre (DCF). Losses are compensated essentially by erbium amplification.

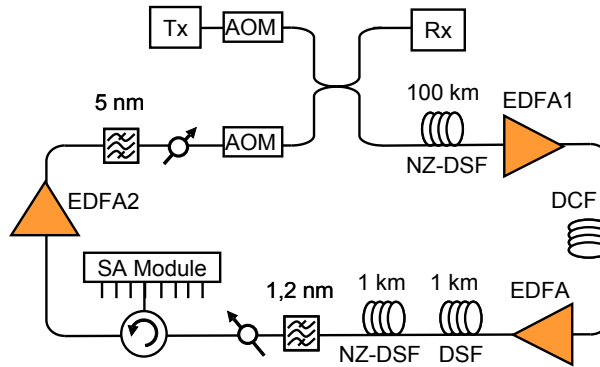


Figure 4: Experimental loop setup for characterization in 2R regeneration configuration.

The passive 2R regenerator is made up of two stages: the first pulse compression stage comprising an optical fibre followed by a filter for equalisation of “mark” levels [5], and the second stage made up of the SA module for extinction ratio enhancement. The fibre in the pulse compression stage consists of 1 km of DSF (dispersion of 0.1 ps/nm/km) and 1 km of NZ DSF (dispersion of 4.5 ps/nm/km). This stage requires an EDFA to ensure a high enough power (typically 18 dBm in our case) to produce significant nonlinear effects. An optical circulator allows the injection and recovery of the data signal from the SA module.

2.3.2 Experimental results

Firstly, the impact of the 2R regeneration was studied at a signal wavelength of 1546.6 nm. Figure 5.(a) presents the bit error rate (BER) evolution as a function of the distance with and without regenerator (full triangles) for a launched power of 5 dBm corresponding to the optimal propagation length. After insertion of the 2R regenerator in the loop, we observe a significant

improvement of the transmission distance for each channel of the SA module. At least 4,000 km are covered with a BER of 10^{-4} for the worst channel.

We have also investigated the regeneration behaviour with respect to the signal wavelength for one channel, channel 5 (Figure 5.b). We measured the distance improvement ratio (DIR) corresponding to the ratio of the distances covered with and without regeneration for a given BER. Results show that the DIR is better than 3 over more than 13 nm (from 1541 nm to 1554 nm), demonstrating experimentally the wide-band behaviour of the device.

These experiments confirm the good homogeneity of the component and its functionality over a wide spectrum. In the context of a WDM configuration, it is possible to process simultaneously 8 channels, with frequency spacing of 100 GHz, with this compact module.

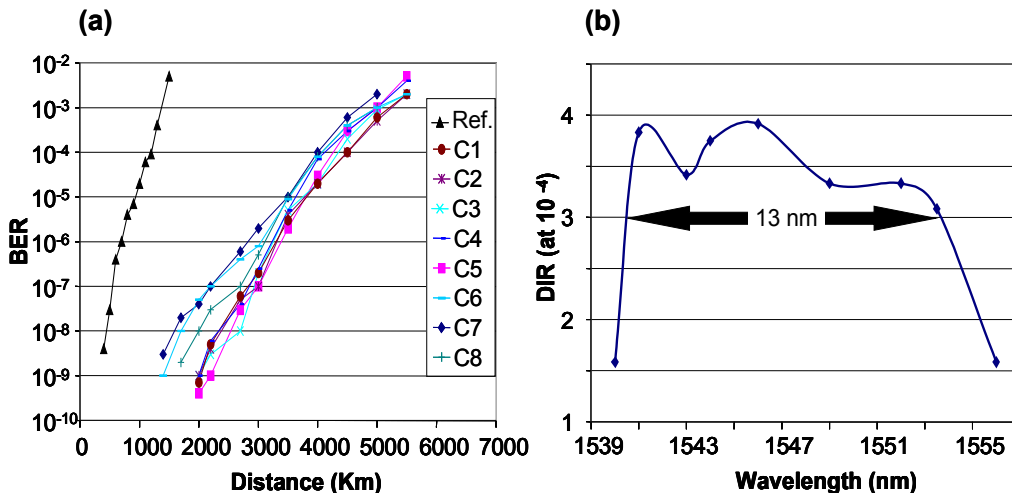


Figure 5: BER evolution versus distance without and with SA module (a) DIR (at $\text{BER}=10^{-4}$) evolution versus signal wavelength for channel 5 (b).

2.4 Conclusion

We have reported for the first time the WDM compatibility of a simple, compact and completely passive 8-channel 2R regenerator module based on a saturable absorber. The SA module average switching contrast is 5.5 dB on all channels and a switching contrast higher than 3 dB is attainable over 18 nm.

We have also shown a distance improvement ratio (at BER of 10^{-4}) of at least 3.3 in a 100-km recirculating loop. Finally, we have demonstrated a distance improvement ratio greater than 3 over 13 nm. This module is fully

compatible with photonic integration, which would allow for a compact and low cost WDM 2R regeneration.

For the moment, the technique for “mark” level equalisation (fibre followed by optical filter) is limiting for WDM application due to inter-channel nonlinearity. Recently, a new design of the same type of nonlinear microcavity device should make it possible to reduce “mark” level fluctuations on several channels simultaneously without the fibre compression stage, and thus all-optical regeneration based on saturable absorption devices is presented in the next section.

3 All-optical 2R regeneration based on saturable absorption

In this section, we report on the regenerative properties of a tandem consisting of a classical SA (SA.0) followed by a new SA structure for power limiting function. The new SA structure, based on the same technology as the SA.0, but with some modification in the cavity parameters, showed promising power limiting, or amplitude fluctuation reduction, capacity and this structure we name “SA.1” [6]. The capacity of the regenerator for noise suppression and Q-factor enhancement, as well as the obtainable sensitivity margin at 42.7 Gbit/s, are presented and discussed.

3.1 Module structure

The structure of the SA.0 used is similar to that of the device used in the previous section. The SA.1 is based on the same structure, but with some parameter modifications to obtain the complementary function to the SA.0. The principle of parameter modifications in the SA.1 structure will be briefly described.

The SA structure consists of several multi-quantum wells (QW) embedded in a microcavity. At the resonance wavelength, the cavity reflection at normal incidence can be expressed as [6]

$$R_{cav} = \left(\frac{\sqrt{R_f} - \sqrt{R_b^{eff}}}{1 - \sqrt{R_f R_b^{eff}}} \right)^2 \quad (1)$$

$$R_b^{eff} = R_b e^{-2\eta NT}$$

where R_f and R_b are the reflectivities of the front and back mirror respectively, R_b^{eff} is the effective back mirror reflectivity accounting for the presence of the QWs, η is the single pass absorption per QW, N is the number of QWs, and Γ is the longitudinal confinement factor. We note that when the incident power increases, the absorbing layers become more transparent (η decreases) which induces an increase in R_b^{eff} . Equation 1 shows that if $R_b^{eff} > R_f$, we have an “increasing” curve of reflectance versus incident power, which is obtained with the usual SA.0 design. On the other hand, the SA.1’s mirror parameters are modified to obtain $R_b^{eff} < R_f$ (Figure 6). As a result, the device reflectance decreases when the incident power increases, giving a power stabilization function.

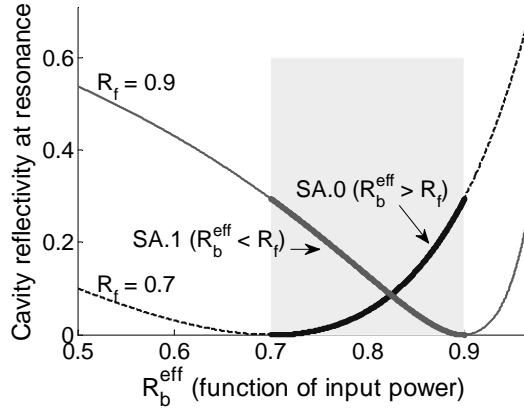


Figure 6: Cavity power reflectivity at the resonance for the cases of SA.0 design (dash line) and SA.1 design (solid line) (Numerical results).

The SA.1 used is composed of 7x(InGaAs-InAlAs) multiple quantum wells, grown by metal-organic vapor-phase epitaxy on an InP substrate and embedded in a microcavity. The QW are suitably located at the antinodes of the intracavity intensity. The back mirror is made by the deposition of a silver layer (with a calculated reflectivity of 0.945), while three pairs of (ZnS-YF₃: $\lambda/4$: $\lambda/4$) are deposited as a top mirror with 0.88 reflectivity. The sample is mounted on a Si substrate by Au-In bonding, to improve heat dissipation and thus to limit thermo-optic effects. In order to reduce the carrier lifetime, the QW are irradiated by 12 MeV Ni⁶⁺ ions with a dose of $4 \cdot 10^{11} \text{ cm}^{-2}$. The 10-MHz pump-probe measurement at 1548 nm showed a response time of 3.4 ps. Table 1 summarizes the parameters of the SA.0 and SA.1 used in this paper.

Table 1: Parameters of the SA.0 and SA.1 used.

Parameters	SA.0	SA.1
QW	7x(InGaAs-InP)	7x(InGaAs-InAlAs)
Substrate	InP	InP
Irradiation	12 MeV Ni ⁶⁺ (10^{12} cm ⁻²)	12 MeV Ni ⁶⁺ ($4 \cdot 10^{11}$ cm ⁻²)
Front mirror	2x[TiO ₂ -SiO ₂]	3x[ZnS-YF ₃]
Rf	0.78	0.88
Back mirror	Ag	Ag
Rb	0.945	0.945
Recovery time	1.5 ps	3.4 ps

3.2 Transfer function

We have then investigated the transfer functions of these SAs. The transfer function is defined as the variation of output power responding to the increase of the input power. Figure 7 displays the average output power and the deduced reflectance of the device versus the average input power for the SA.0 (a) and for the SA.1 (b). The signal is a standard 42.7-Gbit/s RZ-33% signal centred at 1546.6 nm with a 2^7-1 bits PRBS. For the case of SA.0, the device's functionality is such that its reflectance increases in response to high optical powers (above 1 mW). In consequence, this nonlinearity enhances the signal extinction ratio. The SA.1 has, on the contrary, a reflectance which decreases with increasing input power. The relative amplitude fluctuations at the output could be reduced in a large input power range from 2 mW to 20 mW, providing significant amplitude stabilization on the output signal.

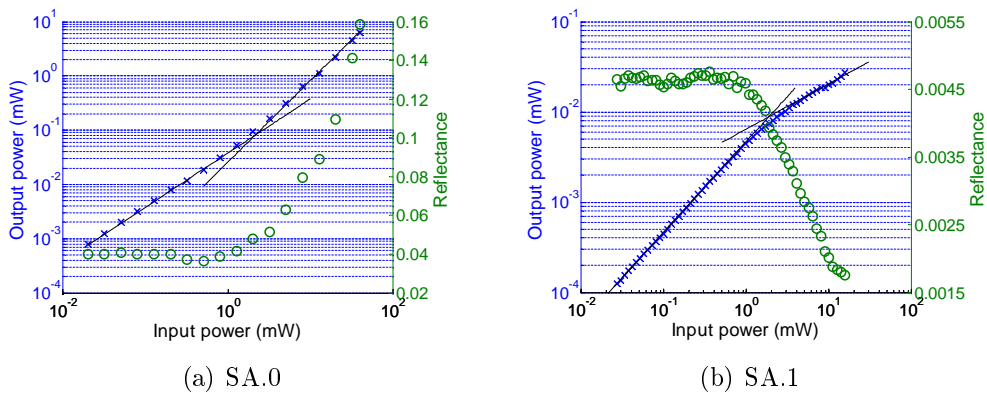


Figure 7: Experimental input-output power transfer functions (crosses) and reflectances (circles) of the investigated devices.

3.3 Back-to-back characterisation

The experimental setup for our 2R regenerator is presented in Figure 8. This is used to characterize the 2R regenerator based on a tandem of SA.0 and SA.1 using a noise-added input signal. The transmitter (Tx) generates a 42.7-Gbit/s RZ-33% signal at 1546.5 nm with a $2^{31}-1$ bits PRBS. Noise produced by an amplified spontaneous emission (ASE) source is added through a 50/50 optical coupler. A 5-nm bandwidth optical filter limits the noise spectrum around the working wavelength. In order to inject a large enough signal power into the SA, the signal is boosted by EDFAs before being sent to the SAs via optical circulators (OC). The tandem, as used, has the SA.0 in the first or input position and the SA.1 placed after this. The optimal power levels were found to be 12 dBm at the SA.0 input and 8 dBm at the input of the SA.1.

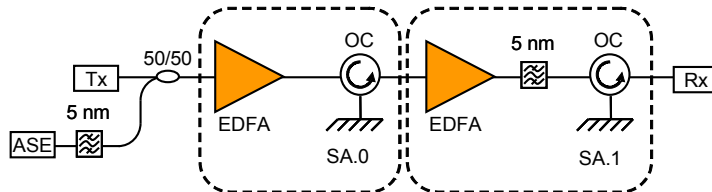


Figure 8: Regenerator structure and experimental setup.

In order to assess how the all-optical 2R changes the noise distribution on the marks and spaces, we first studied the evolution of the BER versus the decision threshold in the electrical receiver. The BER curve provides a direct insight into the noise statistics. The steepness of the flank is representative of intensity fluctuations: the steeper the flank is, the less amplitude noise there is. In the condition of the same average optical powers at the input of the receiver preamplifier, these curves allow comparing the noise distribution of the signal in the cases with 2R and without 2R. Figure 9 depicts the results for an optical signal to noise ratio (OSNR) of 16.7 dB (measured over 1 nm). To begin with, it was carried out without regeneration (diamonds), to give a reference. When the SA.0-SA.1 tandem is used, a significant improvement on both space and mark levels can be observed (Figure 9.a). The Q-factor is improved from 19.2 dB to 20.3 dB due to SA.0-SA.1 regeneration.

In Figure 9.b, we also report the eye diagrams with and without regeneration, as obtained with an optical sampling oscilloscope (resolution of 1 ps) and for the same signal input power. While the presence of noise and the observation of noise distribution improvement are not clearly evident here, we do notice that the tandem regeneration function does not distort the RZ

pulse shape. Indeed, the improvement of noise distribution is not really noticeable on the eye diagram after one passage, but can be clearly observed after several cascades of this regenerator in a recirculating loop.

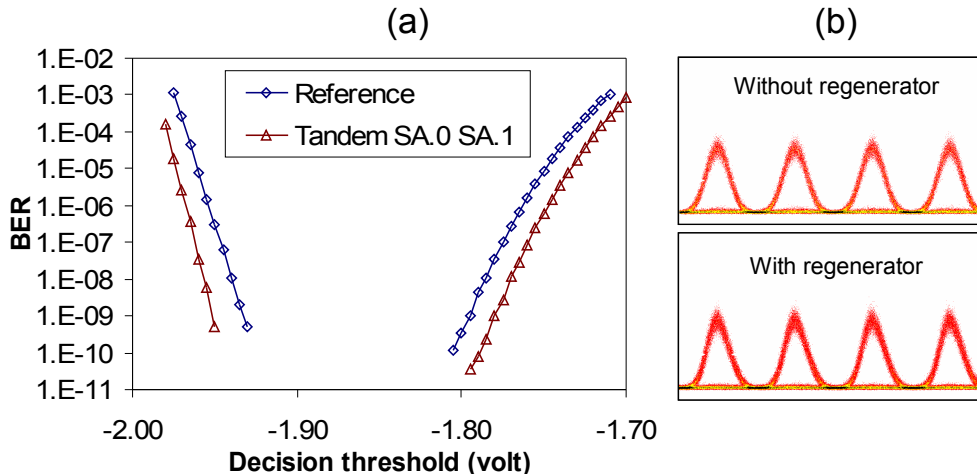


Figure 9: BER versus decision threshold (a) and eye diagram (b) w/o and with regeneration. OSNR= 16.7 dB in 1 nm.

3.4 Recirculation loop characterisation

The SA.0-SA.1 tandem has been tested in a recirculating loop. The loop was composed of a short length of DSF (10 km) in order to assess the cascability of the regenerator independently from the propagation effects. The experimental setup is shown on Figure 10. The transmitter (Tx) produces an RZ-33% optical signal modulated at 42.7 Gbit/s with a $2^{31}-1$ bits PRBS at 1550 nm. An optical filter limits the ASE accumulation over the full amplification band. The signal was injected into the SA using optical circulators (OC). The ASE noise was added into the loop to assess the tandem's ability to reduce it. With noise, the OSNR was equal to 18 dB (over 1 nm) after one cascade without regeneration and a BER of 10^{-8} was obtained after 4 cascades.

When the tandem SA.0-SA.1 is included, an optimum operation was obtained with an input power of 10 dBm at the input of the SA.0 and 9 dBm at the input of the SA.1. A transmission over 10 cascades with a BER of 10^{-8} is achieved. We have thus demonstrated an increase of the number of cascades by a factor of 2.5. Figure 11 shows the eye diagrams after 10 cascades, with and without regenerator, showing the noise reduction on mark level.

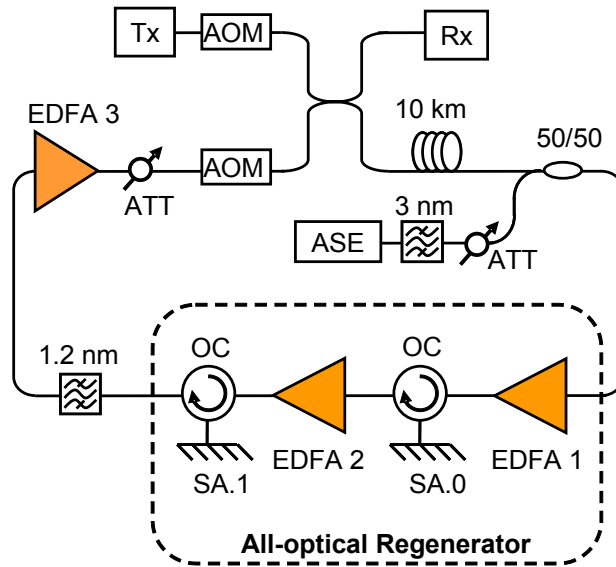


Figure 10: SA.0-SA.1 tandem in a recirculating group.

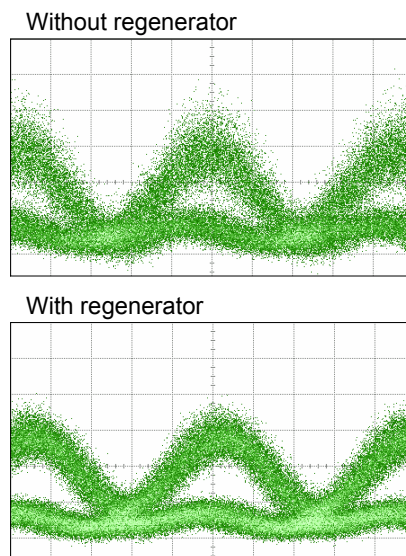


Figure 11: Signal eye diagram after 10 laps w/o and with regeneration.

However, some efforts still have to be made on the SA.1 and on the regenerator architecture as it was found impossible to properly cascade the regenerator more than 10 times. Some spectral deformations are the principal limitation. The saturation of the absorption gives rise to a dip in the reflectivity spectrum; hence the signal spectrum is distorted when transmitted through the device, in a cumulative way. We should, however, be able to compensate for this effect with a gain equalizer filter.

4 Study of an optical 3R regenerator based on saturable absorber

Here, we report the cascability assessment of a 3R regeneration device based on a 2R regenerator and all-optical synchronous modulation. The 2R regenerator is based on the combination of self-phase modulation (SPM) in an optical fibre and Saturation Absorption (SA) in a quantum-well microcavity. The all optical synchronous modulation is achieved by launching into the SA the optical clock obtained from an all optical clock recovery device using self-pulsating (SP) semiconductor lasers based on bulk and quantum-dot (QD) structures.

4.1 Regenerator architecture

Figure 12.(a) presents the regenerator architecture. The passive 2R regenerator is the one presented in Section 2, which is made up of two stages: the first pulse compression stage comprising an optical fibre followed by an optical band-pass filter (OF), for equalisation of “mark” levels. This stage requires an EDFA with 18 dBm output power. The second one is made up of the SA module for extinction ratio enhancement.

The optical clock recovery (OCR) part is implemented to introduce the synchronous modulation. Our OCR consists of a double stage SP laser from Alcatel Thales III-V lab (Figure 12.(b), previously described in [7]. The first stage is a distributed Bragg reflector (DBR) laser, containing a polarization insensitive bulk active layer. The second one is a quantum-dot Fabry-Perot laser (QD). The first laser produces an optical clock at 1548 nm which is precisely synchronized to the optical data signal at the input at 42.7 GHz. The great advantage of this laser is its polarisation insensitivity. The second one works at 1575 nm and provides a high purity clock thanks to its intrinsic jitter filtering effect. The association of these two lasers yields a polarisation insensitive high performance OCR component.

The optical clock is then injected to the transmission line and launched into the SA. The relative delay between incoming data and recovered clock can be controlled by an optical delay line (ODL). The optical synchronous modulation is obtained by cross absorption modulation in the SA. The optical clock is then filtered out of the transmission line by the second filter.

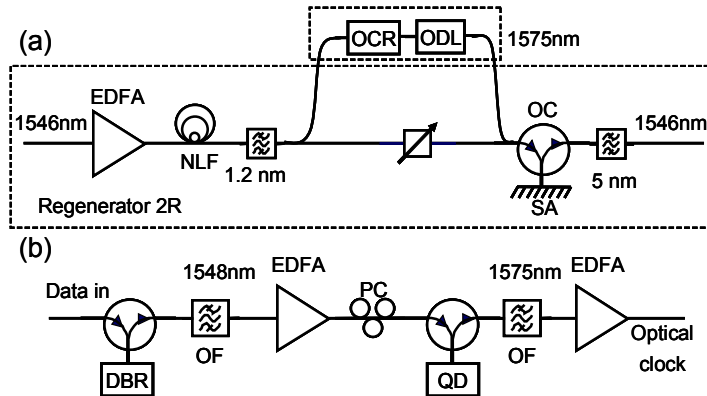


Figure 12: Regenerator architecture (a), and optical clock recovery part (b).

4.2 Cascadability experiment

The recirculating loop setup is shown in Figure 13. The transmitter produces an RZ (33%) optical signal modulated at 42.7 Gbit/s with a PRBS sequence length of $2^{31}-1$.

The transmission loop consists of 100 km of TrueWave Reduced Slope (TW-RS) fibre with a chromatic dispersion of 4.5 ps/nm/km at 1550 nm. Distributed Raman amplification is achieved by backward pumping of the transmission fibre. The on/off Raman gain for each span is approximately 10 dB. The chromatic dispersion is compensated for, just before the regenerator, by an enhanced high slope DCF module.

Figure 14 shows the BER as a function of transmission distance with and without synchronous modulation. Without the synchronous modulation, using only 2R regeneration, the BER grows rapidly due to timing jitter. However, BER of 10^{-8} is attainable over 8,000 km corresponding to a factor 10 of transmission distance enhancement as compared to the case without regeneration.

When the optical synchronous modulation is included, the timing jitter is reduced and the transmission distance is considerably improved. At a BER of 10^{-8} , a distance of 18,000 km is attainable with corresponding to a transmission distance improvement factor of 22.5.

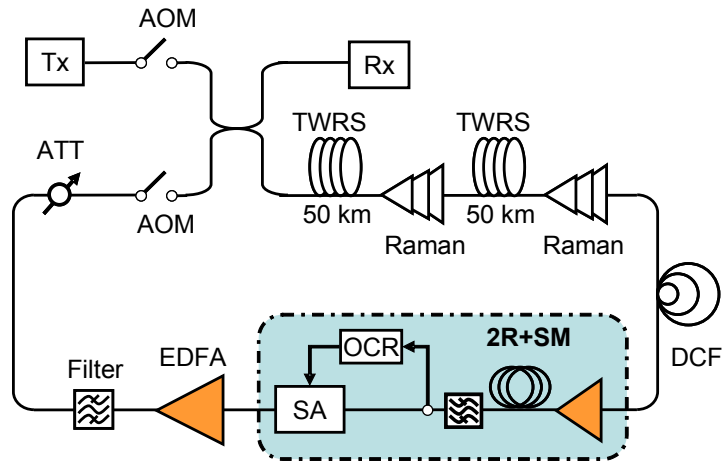


Figure 13: Schematic of the recirculation loop experiment. The 100 km loop consists of two spans of 50 km TWRS fibre, DCF and an Optical 3R regenerator.

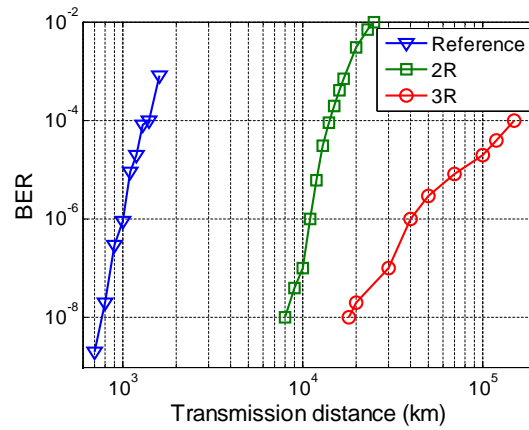


Figure 14: BER as a function of transmission distance.

Reduction of timing jitter can be observed by measurements of the evolution of BER versus decision time (Figure 15). We observe a significant margin on receiver decision time with synchronous modulation case at 90,000 km in comparison with the 2R regeneration case at 13,000 km. Consequently, we have demonstrated the efficiency of the optical synchronous modulation obtained by cross absorption modulation in the SA.

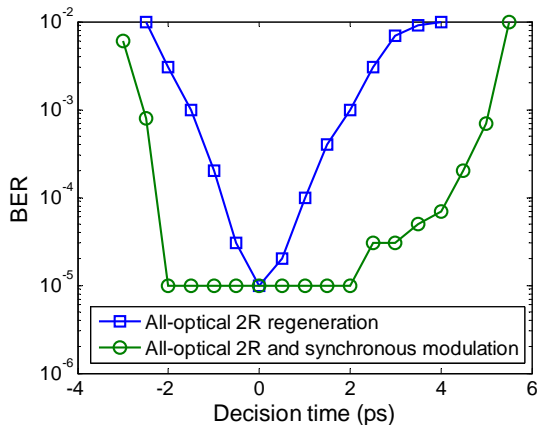


Figure 15: BER versus decision time.

However, we do not observe a classical BER evolution versus distance for 3R inline regeneration. Theoretically, the BER increases linearly with cascade number (N) of the regenerator [8]:

$$BER = N.exp(-k.OSNR) \quad (2)$$

OSNR is measured at the input of the regenerator, k is a system constant.

We have performed a numerical simulation which shows that the principal limitation is due to the strong timing jitter. This timing jitter is generated by the soliton effect in fibre-based 2R regenerator (known as Gordon-Haus effect). Indeed, in the fibre-based power limiter, the intensity noise is converted into instantaneous frequency fluctuations by SPM. With the chromatic dispersion, these instantaneous frequency fluctuations lead to arrival time fluctuations of the pulses. Combining with the synchronous modulation, which is an over-modulation of the signal intensity, a pulse will be completely attenuated if its position is too far from the bit centre. As a result, the regenerator creates an error at the receiver. The Gordon-Haus timing jitter increases with an increase of ASE noise. The probability of pulse attenuation is thus increased with ASE noise. To overcome the Gordon-Haus limit, a new 2R regenerator design using saturable absorption devices (as presented in Section 3) could be used to replace the fibre-based one.

4.3 Conclusions

Thanks to an experimental cascability assessment study, we have shown for the first time the efficiency of an all optical synchronous modulation regenerator using cross absorption modulation in a SA microcavity, and a very compact clock recovery. We show a considerable improvement in propagation distance at 42.7 Gbit/s. A significant margin on receiver decision time is obtained with this modulation technique showing evidence of a retiming effect. Finally, this all optical signal regeneration technique could be improved in the future by using a newly designed SA microcavity for better “mark” regeneration, which could avoid using the fibre nonlinearity.

5 Saturable absorber for phase preserving amplitude regeneration of an RZ DPSK signal

Phase-shift keying (PSK) is a strong candidate for high-capacity ultra-long-haul optical systems and has therefore been widely studied. This trend has driven the search for all-optical PSK signal regeneration in order to improve the transmission quality of these systems.

The reach of an optical PSK transmission is mainly limited by the accumulation of linear and nonlinear phase noise. Linear phase noise results from amplified spontaneous emission (ASE) in optical amplifiers. Nonlinear phase noise (NLPN) results from intra- and inter-channel nonlinearities such as self phase modulation (SPM) (i.e. the Gordon-Mollenauer effect) and cross phase modulation (XPM) that convert amplitude noise to phase noise. By increasing the launched channel power, the impact of the linear phase noise induced by the accumulation of ASE can be reduced. However, the nonlinear phase noise then becomes the most critical impairment factor.

Some recent work focused on phase noise reduction using an interferometric phase-sensitive amplifier; an experimental demonstration of phase and amplitude regeneration has been reported [9]. Phase-regenerative amplification of a DPSK (Differential PSK) signal suffering only phase noise has been demonstrated in a combined Sagnac-SOA structure [10]. Moreover, phase-preserving amplitude regeneration can prevent the accumulation of NLPN during transmission [11]. Some techniques based on four-wave mixing in fibre [12] and on a nonlinear optical loop amplifier [13] have been experimentally investigated.

Recently, a new generation of multiple-quantum-well saturable absorber allowing power stabilization (called SA.1) has been developed [6]. As shown in Section 3, this new structure, when associated with the classical sat-

urable absorber (SA), which allows extinction ratio improvement, has shown good performance for all-optical amplitude-shift-keying signal regeneration. Thanks to its very thin structure (on a hundred-nanometer scale), the induced chirp, given by the Kramers-Krönig relations, is low. Consequently, phase variations of the signal reflected by the SA chip are almost unchanged. In the context of return-to-zero differential phase-shift keying (RZ DPSK) signal regeneration, the SA.1 can thus be used for phase-preserving amplitude regeneration, hence preventing NLPN accumulation at high launched channel power. The device is fully passive, requiring neither a Peltier cooler nor a bias voltage, and promises a compact and WDM-compatible solution (simultaneous processing of several tens of channels on 1 mm²).

In this work, we report on a novel all-optical phase-preserving amplitude regeneration technique for RZ DPSK signals in which the amplitude fluctuations are reduced by the use of a SA.1. Nonlinear phase noise reduction is studied with BER and Q-factor measurements.

5.1 Experimental setup and principle of operation

The experimental scheme aims at demonstrating the device efficiency in realistic working condition. The regenerator is located where the signal is already corrupted by amplitude noise but where the NLPN amount is not high enough to severely degrade the system performance. To achieve this, the optical OSNR at the transmitter is degraded and a high channel power is used (Figure 16). By strongly reducing the amplitude noise, the SA.1 prevents the accumulation of NLPN in the next transmission span.

The transmitter (Tx) generates an 8-ps-pulse-width RZ DPSK signal at 42.7 Gbit/s by using two Mach-Zehnder modulators, one for pulse carving and the other in a push-pull arrangement for phase coding. The signal wavelength is centred at 1550 nm. To achieve OSNR degradation before transmission, an ASE source followed by a 3-nm band-pass optical filter, centred on the working wavelength, and an optical attenuator (ATT) are used. The signal is boosted to 6 dBm by an EDFA1 before being sent to the SA.1 via an optical circulator (OC). The transmission fibre is a NZ DSF with a chromatic dispersion of 4.5 ps/km/nm at 1550 nm followed by a length of DCF. EDFA2 is used as a power booster to obtain a signal power, launched into the transmission fibre, of up to 18 dBm. EDFA3 compensates the residual loss. The pre-amplified RZ DPSK receiver (Rx) consists of a fibre-based delay-line interferometer for demodulation of the DPSK signal and a balanced detector.

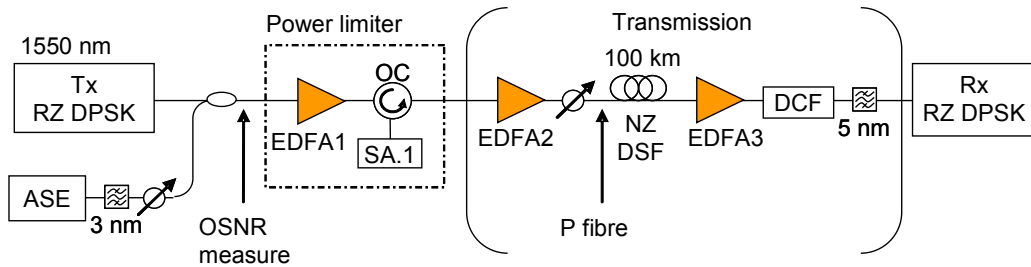


Figure 16: Experimental setup.

5.2 Experimental results and discussion

Figure 17 shows the measured BER versus the receiver input power. The first curve (rhombi) refers to the case of back-to-back reception (no transmission and without regeneration) without added noise (good OSNR: 30 dB). The square-mark curve is the case of back-to-back with an OSNR at the transmitter of 13.8 dB. The BER in this case is mainly limited by the linear phase noise induced by the ASE source. The triangle-mark curve refers to a transmission case with 16 dBm launched power and without power limiting. A large power penalty is observed and an error floor at a BER of $5 \cdot 10^{-10}$ appears, owing to linear and nonlinear phase noise. When the SA.1 based amplitude regenerator is used, the amplitude fluctuation is reduced, and NLPN is partly removed. We obtain a considerable improvement of the BER for the same fibre launch power (circle-marked curve). Indeed, the BER curve with regeneration is brought close to the one limited only by linear phase noise, with the result that the error floor disappears from the measurable range of BER. The efficiency of the regenerator is thus demonstrated.

Signal improvement by the SA.1 is also investigated via Q-factor measurements. The Q-factor is evaluated using the Gaussian approximation. Figure 18 shows the Q-factor versus signal power launched into the 100-km fibre span for an initial OSNR of 17.4 dB (full-mark curves) and 11.8 dB (empty-mark curves). The square-mark curves and the triangle-mark curves refer to the cases with and without SA.1 respectively. When the OSNR equals 17.4 dB, we observe clearly the Q-factor degradation due to NLPN as the signal power exceeds 15 dBm. In the case with SA.1 based regeneration, this degradation is reduced (for longer transmission distances, the Q-factor curves would be shifted to lower input power values since less launched power is needed for the same amount of total NLPN in the system). For signal powers less than 15 dBm, the nonlinear phase noise is negligible compared to the linear phase noise. As a consequence, the Q-factor cannot be improved by

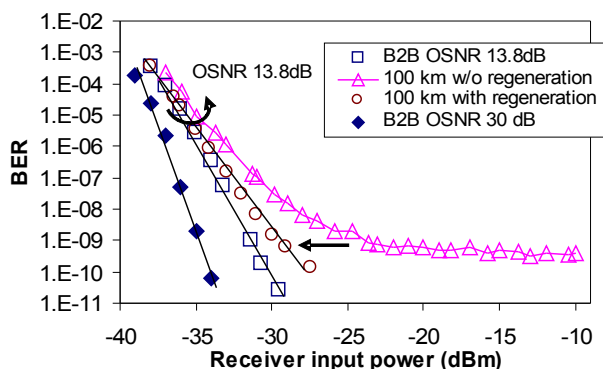


Figure 17: BER of the RZ DPSK signals versus receiver input power for an OSNR at the transmitter of 13.8 dB.

SA.1 which preserves the linear phase noise accumulation. The greater the signal power, the greater the nonlinear conversion effects, and thus the better the Q-factor improvement, due to the SA.1. The Q-factor is improved by 2 dB at 17.8 dBm signal power.

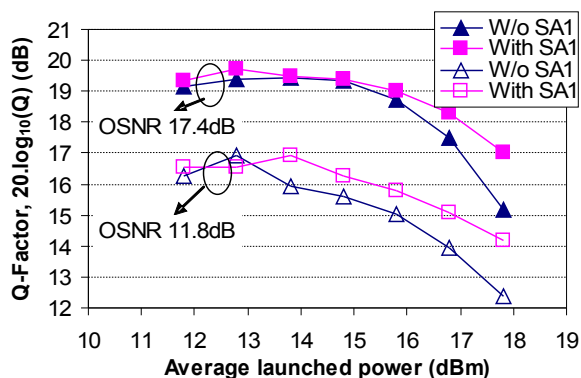


Figure 18: Dependence of demodulated electrical Q-factor on the launched power into the transmission fibre.

When the signal is more degraded (OSNR of 11.8 dB), the SA.1 is effective for a launched power exceeding 13 dBm, compared to 15 dBm in the previous case. This can be explained by the fact that when more amplitude noise is added to the signal, the transfer of amplitude noise into phase noise by nonlinear effects increases, and thus the efficiency of the SA.1 appears at lower signal power. A Q-factor improvement from 1 dB to 2 dB is obtained when the signal power increases from 14 dBm to 18 dBm in this case.

5.3 Recirculating loop experiment

The experimental setup is shown in Figure 19. The transmitter generates an 8-ps-pulse-width RZ DPSK signal at 42.7 Gbit/s. The signal wavelength is centred at 1550 nm. An ASE source followed by a 3-nm band-pass optical filter, centred at 1550 nm, followed by a variable optical attenuator (ATT) is used in order to modify the OSNR at the transmitter output.

The signal is boosted by EDFA1 before being sent to SA.1 via an optical circulator (OC). The transmission line consists of 100 km of NZ DSF with chromatic dispersion of 4.5 ps/km/nm at 1550 nm, followed by a DCF. EDFA2 increases the launched power up to 13 dBm, while EDFA3 compensates for the residual loss. A gain equalizer (EG) is required to compensate for the signal spectrum distortion due to the SA.1's resonance. The pre-amplified RZ DPSK receiver consists of a fibre-based delay-line interferometer and a balanced detector.

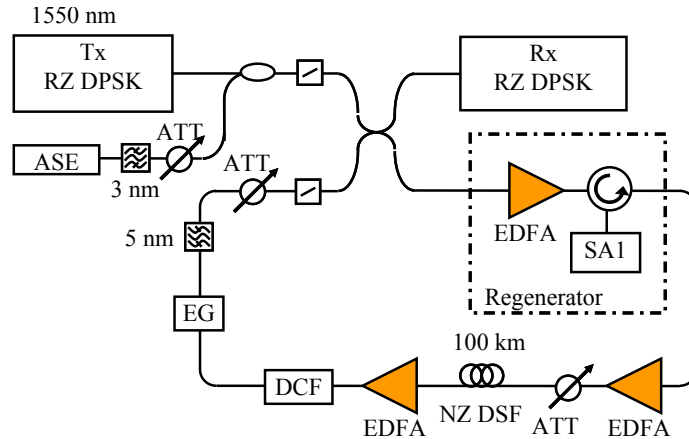


Figure 19: Experimental setup.

5.4 Experimental results

Figure 20 shows the measured BER versus transmission distance with and without SA.1 based amplitude regeneration. The OSNR at the transmitter (called $OSNR_{Tx}$) is 22.7 dB (over 1 nm) and the fibre launched power is 13 dBm. This high value is unrealistic, but it allows us, in our experiment, to generate a high enough amount of NLPN in 100 km of transmission fibre. For longer distance between regenerators, the BER curves will be shifted towards lower input power values since less launched power is needed for the same amount of total nonlinear phase noise in the system. In the case

without SA.1, the BER grows rapidly due to linear and nonlinear phase noise accumulation. When the phase-preserving amplitude regenerator is included, the amplitude noise is reduced and the NLPN is partly removed. As a consequence, the transmission distance is enhanced thanks to the regenerator. A transmission distance of 800 km is reached for a BER of 10^{-4} compared to 500 km in the case without regeneration, a distance improvement ratio of 1.6 is thus obtained.

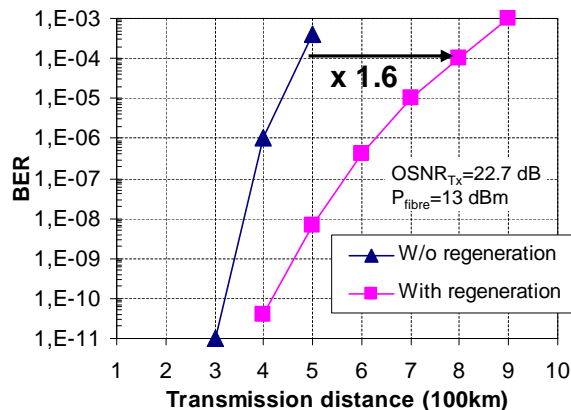


Figure 20: BER versus transmission distance ($\text{OSNR}_{Tx}=22.7$ dB, $P_{\text{fibre}}=13$ dBm).

We define the distance improvement ratio (DIR) as the ratio of distances covered with and without regeneration for a given BER. Figure 21 presents the evolution of DIR versus OSNR_{Tx} at the transmitter for a BER of 10^{-4} and with fibre launched powers of 10 dBm and 13 dBm. The results show that the DIR generally exceeds 1.2 for all OSNR_{Tx} values. As can be seen, a difference in regeneration efficiency is shown when the fibre launched power varies from 10 dBm to 13 dBm. This can be explained by the fact that, at higher fibre launched power (13 dBm), the nonlinear effects that convert amplitude noise into phase noise are greater. Consequently, better regenerator efficiency is obtained (distance improvement ratio of 1.4 to 1.6 compared to 1.2 at 10 dBm). The greater the fibre launched power, the greater the nonlinear conversion effects are, and therefore the better the distance improvement obtained with the SA.1 are.

When OSNR_{Tx} increases the obtained DIR is slightly better. For a fibre launched power of 13 dBm, a DIR of 1.4 is obtained at low OSNR_{Tx} (13.8 dB), and this improvement ratio is 1.6 at high OSNR_{Tx} (22.7 dB). At a fibre launched power of 10 dBm, this evolution is less visible because the nonlinear effects are less present.

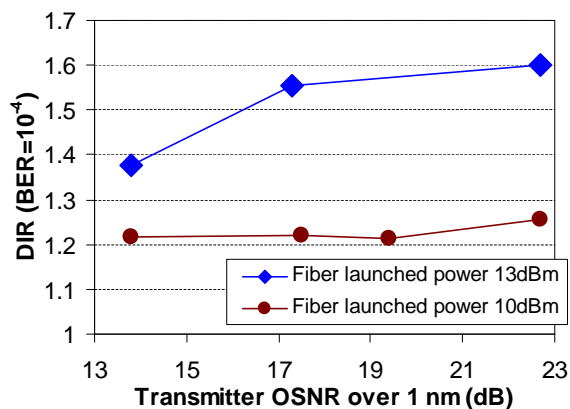


Figure 21: Distance improvement ratio versus transmitter OSNR.

5.5 Conclusions

We have reported for the first time the efficiency of the power-limiter saturable absorber for the regeneration of high-power RZ DPSK signals. The device reduces the amplitude fluctuations while preserving the signal phase, hence preventing the generation of nonlinear phase noise. The BER and Q-factor measurements show the obtained signal quality improvement at high signal power where the nonlinear phase noise is significant. A Q-factor improvement up to 2 dB is obtained.

Cascaded performance of the device has been experimentally investigated in a 42.7-Gbit/s RZ-DPSK transmission system via a recirculating loop setup. The results obtained show that the regenerator reduced the amplitude noise, which is the origin of nonlinear phase noise, thus improving the system performance. The best regenerator efficiency is achieved at high fibre launched power where the nonlinear effects are significant. A distance improvement ratio of up to 1.6 is experimentally obtained.

References

- [1] D. Massoubre, J. Oudar, G. Aubin, J. Dion, A. Shen, N. Lagay, J. Decobert, A. O'Hare, Z. Belfqih, M. Gay, L. Bramerie, S. Feve, E. Le Cren, and J.-C. Simon, "High speed, high switching contrast quantum well saturable absorber for 160 Gbit/s operation," in *Conference on Lasers and Electro-Optics*, Baltimore, Maryland, 2005, p. CThD3.

- [2] A. Shen, M. Goix, S. Louis, D. Delagrèdière, J. Decobert, G. Henin, D. Rouvillain, O. Leclerc, H. Choumane, G. Aubin, and J.-L. Oudar, “4-channel Saturable Absorber Module for high bit-rate regenerated WDM transmission,” in *European Conference on Optical Communications*, Copenhagen, Denmark, 2002, p. Tu 5.4.5.
- [3] M. Gay, L. Bramerie, J.-C. Simon, A. O’Hare, D. Massoubre, J.-L. Oudar, and A. Shen, “Cascadability and wavelength tunability assessment of a 2R regeneration device based on saturable absorber and semiconductor optical amplifier,” in *Optical Fiber Communication Conference*, California, USA, 2006, p. OThB1.
- [4] D. Massoubre, J.-L. Oudar, J. Dion, J. Harmand, A. Shen, J. Landreau, and J. Decobert, “Scaling of the saturation energy in microcavity saturable absorber devices,” *Appl. Phys. Lett.*, vol. 88, p. 153513, 2006.
- [5] M. Matsumoto and O. Leclerc, “Analysis of 2R optical regenerator utilising self-phase modulation in highly nonlinear fibre,” *Electron. Lett.*, vol. 38, pp. 576–577, Jun. 2002.
- [6] H. T. Nguyen, J. Oudar, S. Bouchoule, G. Aubin, and S. Sauvage, “A passive all-optical semiconductor device for level amplitude stabilization based on fast saturable absorber,” *Appl. Phys. Lett.*, vol. 92, p. 111107, 2008.
- [7] B. Lavigne, J. Renaudier, F. Lelarge, O. Legouezigou, H. Gariah, and G. Duan, “First demonstration of a polarization insensitive low time jitter and optical noise tolerant all-optical clock recovery at 40 GHz using a self-pulsating laser tandem,” in *Optical Fiber Communication Conference*, Anaheim, California, 2006, p. PDP24.
- [8] P. Ohlen and E. Berglind, “Noise accumulation and BER estimates in concatenated nonlinear optoelectronic repeaters,” *IEEE Photonics Technol. Lett.*, vol. 9, no. 7, pp. 1011–1013, 1997.
- [9] K. Croussore, C. Kim, Y. Han, I. Kim, and G. Li, “All-optical phase and amplitude regeneration of DPSK signals based on phase-sensitive amplification,” in *Optical Fiber Communication Conference*, Anaheim, California, 2006, p. OFH7.
- [10] P. Devgan, M. Shin, V. Grigoryan, J. Lasri, and P. Kumar, “SOA-based regenerative amplification of phase noise degraded DPSK signals,” in *Optical Fiber Communication Conference*, Anaheim, California, 2005, p. PDP34.

- [11] S. Boscolo, R. Bhamber, and S. Turitsyn, "Design of Raman-Based Nonlinear Loop Mirror for All-Optical 2R Regeneration of Differential Phase-Shift-Keying Transmission," *IEEE J. Quantum Electron.*, vol. 42, no. 7, pp. 619–624, 2006.
- [12] M. Matsumoto, "Nonlinear phase noise reduction of DPSK signals by an all-optical amplitude limiter using FWM in a fiber," in *European Conference on Optical Communications*, Cannes, France, 2006, p. Tu1.3.5.
- [13] K. Cvecek, G. Onishchukov, K. Sponsel, A. Striegler, B. Schmauss, and G. Leuchs, "Experimental investigation of a modified NOLM for phase-encoded signal regeneration," *IEEE Photonics Technol. Lett.*, vol. 18, no. 17, pp. 1801–1803, 2006.